
PREDICTED EMBEDDING POWER REGRESSION FOR LARGE-SCALE OUT-OF-DISTRIBUTION DETECTION

Hong Yang, William Gebhardt, Alexander G. Ororbia*, and Travis Desell*

Rochester Institute of Technology
1 Lomb Memorial Dr, Rochester, NY 14623
[hy3134 wdg1351, agovcs, tjdvse]@rit.edu

ABSTRACT

Out-of-distribution (OOD) inputs can compromise the performance and safety of real world machine learning systems. While many methods exist for OOD detection and work well on small scale datasets with lower resolution and few classes, few methods have been developed for large-scale OOD detection. Existing large-scale methods generally depend on maximum classification probability, such as the state-of-the-art grouped softmax method. In this work, we develop a novel approach that calculates the probability of the predicted class label based on label distributions learned during the training process. Our method performs better than current state-of-the-art methods with only a negligible increase in compute cost. We evaluate our method against contemporary methods across 14 datasets and achieve a statistically significant improvement with respect to AUROC (84.2 vs 82.4) and AUPR (96.2 vs 93.7).

1 Introduction

Out of distribution (OOD) detection is a critical tool for the development of safe and reliable autonomous and semi-autonomous machine learning (ML) systems. Identification of anomalous inputs allows intelligent systems to initiate a conservative fallback policy or to defer to human judgment, reducing the risks to all stakeholders. Hendrycks [14] noted that OOD detection is important for safety critical systems, such as self-driving cars and detecting novel microorganisms. As a result, a plethora of literature has emerged over the years for addressing the problem of OOD detection [2, 15, 16, 22, 25]. However, these efforts focus on small and lower resolution datasets. Although, recent work has attempted to address the issue of large scale OOD detection [13, 18] on large datasets at high resolution [8, 33].

Emerging safety critical systems operate on a much larger dataset at much higher resolutions, the real world. Unlike small datasets, real world data often contains hundreds or thousands of classes at a very high resolution. Use cases for OOD detection range from autonomous driving [3] to medical imaging [29], applications that contain a significant number of potential classes. However, the reliability of the typical baseline OOD detection method [15] decreases rapidly as the number of classes increases, resulting in a change from 17.3% false positive rate at 95% true positive rate (FPR95) with 50 classes to a 76.9% FPR95 when using 1000 classes [18].

Our research is motivated by the need to improve OOD detection methods for use in safety critical applications. We focus on the theoretical concept of Bayesian conditional probability for improving the decision boundary between in-distribution and OOD data. If we consider softmax classification as estimating the class y given data x as $P(y|x)$, our method considers modeling $P(x|\hat{y})$, the probability of the data given the predicted class itself. Doing so will allow us to further consider the marginal probability of $P(\hat{y})$ existing within our in-distribution data, leading us to develop an efficient and effective method for scoring OOD data.

We estimate $P(\hat{y})$ by leveraging the behavioural characteristics of the exponential linear unit (ELU) [6] activation function and the process of batch normalization [19]. Notably, we find that combining the ELU function with batch normalization results in sparse, large values for an embedding z prior to the final classification layer for in distribution data. A large expected embedding value $\mathbb{E}(z|\hat{y})$ functions as a proxy for $P(\hat{y})$, such that larger expected embedding values indicate a \hat{y} that has been observed repeatedly during training, see Figure 3.

*Equal advising.

We extensively evaluate our approach on models trained with the Imagenet 1k dataset [8], leveraging the state-of-the-art pre-trained BiT-S models [21] as our pre-trained model backbone. We significantly reduce required computation and memory usage by pre-computing our backbone outputs and demonstrate that our efficient approach successfully reproduces the results from [18], the state-of-the-art large-scale OOD detection task on Imagenet 1K. Compared to the previous best method [18], we demonstrate that our method scores higher in terms of area under the receiver operating characteristic (AUROC) curve (84.2 versus 82.4) and area under the precision-recall (AUPR) curve (96.2 versus 93.7) on a larger, more diverse set of benchmarks. The results of this paper mark an important step towards leveraging the conditional probability of intermediate outputs for OOD detection. Below, we summarize this study’s **key results and contributions**:

- We propose a novel conditional probability-based scoring method, the Predicted Embedding Power Regression (PEPR) method and the Combined PEPR (C-PEPR) method, that performs better than current state-of-the-art by a statistically significant margin.
- We introduce a high variance OOD detection method that benefits from ensembling. Contemporary methods tend to exhibit extreme stability across runs for all measured performance metrics. In contrast, our approach’s stochasticity results in ensembling benefits.
- We reproduce contemporary methods across a larger group of benchmarks and demonstrate that our computational method is more energy and compute efficient, reducing the training step time by nearly 80%. Unlike previous papers, our experiments measure the standard deviation across multiple runs and establish a statistically significant improvement over the state of the art.

2 Related Work

Multi-class OOD Detection with Pre-trained Models: A common baseline for OOD was historically established by Hendrycks and Gimpel [15] which specifically used the maximum softmax probability. Further efforts have attempted to improve the OOD estimation by using the ODIN score [25], deep ensembles [22], a Mahalanobis distance-based confidence score [24], Energy score [26], as well as the Minimum Other Score [18]. Note that these methods do not use any OOD data for fine tuning or training.

Multi-class OOD Detection with Model Fine-tuning: An alternative research direction is to leverage additional data from outside of the distribution in order to regularize the model [2], [11], [28]. In this setup, additional/auxiliary data may be realistic images [16] or synthetic images generated by generative adversarial networks (GANs) [23]. These extra images are used in various ways, such as to regularize the probabilities back to a uniform distribution [23] or as “background” class samples [30]. Note that constructing additional OOD data assumes a distribution for such data points. This means that the additional OOD data may not be similar to other OOD data samples that the model would encounter in the wild.

Large Scale Multi-class OOD Detection: This line of work focuses on datasets with a large number of classes, most commonly found in Imagenet 1k. [34] utilized half of Imagenet 1k as in-distribution data and the other half as out-of-distribution data. They also used the Places-434 dataset and evaluated a plethora of different approaches, including KL matching and MSP. [18] introduced a grouped cross-entropy to generate an implicit inter-group background class, which was demonstrated to improve system performance. [13] further increased the number of classes by using data from Imagenet 21k.

Hierarchical Classification: Hierarchical structure can provide additional label information, which can facilitate efficient inference [9], improved generalization accuracy [7], and better object detection [32]. Some efforts have made use of a label tree structure when a taxonomy is unavailable [7, 9]. Many studies explore the benefits and importance of basic hierarchical structures for various classification tasks [12, 17, 36].

Bayesian Randomised MAP Sampling: This line of related work exploits the fact that adding a regularisation term to a loss function returns a maximum a posteriori (MAP) parameter estimate, i.e., a point estimate of the Bayesian posterior. Repeating this calculation produces a distribution of MAP solutions that mimicks that of the true posterior. This allows for efficient sampling of high-dimensional posteriors [4]. Some methods allow for sampling of the posterior but fail to recover the true posterior itself [27]. In contrast, other methods require significant computational resources for recovering the true posterior [1]. Work done in [31] provided a suitable compromise with respect to the accuracy of the posterior and an increase in computational cost.

3 Methodology

3.1 Preliminaries

We consider a training dataset drawn i.i.d. from the in-distribution P_X , with label space $Y = 1, 2, \dots, C$. For the OOD detection problem, we train a classifier $F(x)$ on the in-distribution P_X , and evaluate it on samples that are drawn from a

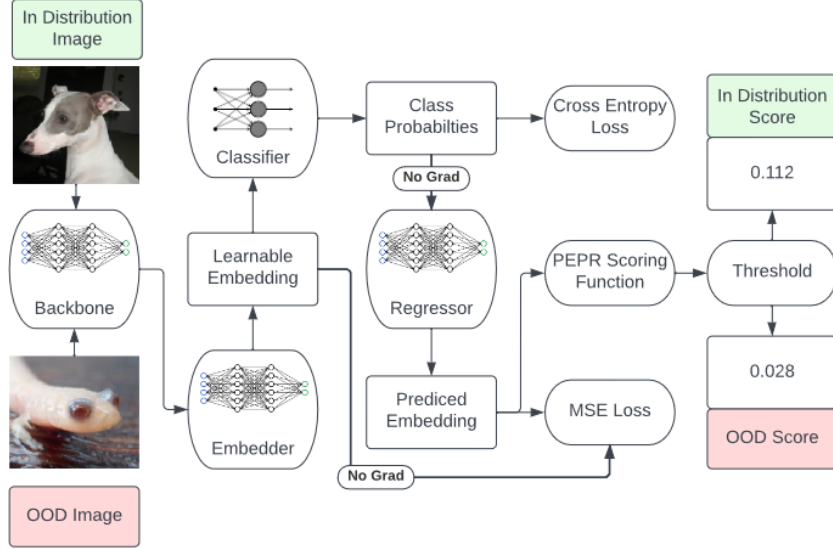


Figure 1: Overview of the PEPR model. The process consists of the following steps: **(1)** Learn to classify training images via the learnable embedding, **(2)** Estimate the embedding values conditioned on the predicted class probabilities, and **(3)** Define a threshold and use PEPR to calculate the score. No gradient flows between parts **(1)** and **(2)** and no OOD images are used during training. Note that the classifier can be any fully connected layer, depending on the number of classes. Definitions for the embedder and regressor can be seen in listings 1 and 2

different (outside) distribution Q_X . An OOD detector $G(x)$ is a binary classifier defined as:

$$G(\mathbf{x}) = \begin{cases} 1 & \text{if } S(\mathbf{x}) \geq \gamma \quad // \text{“in”} \\ 0 & \text{if } S(\mathbf{x}) < \gamma \quad // \text{“out”} \end{cases} \quad (1)$$

where $S(x)$ is a scoring function and γ is a threshold, determined by the target practical application of the OOD detector (different applications would have different precision and recall targets).

3.2 KL Matching and Class Similarity

KL matching [13] provides a useful intuition for solving large scale OOD detection. As the number of classes/categories increases, the similarity between classes may also increase, leading to reduced confidence in the classifier’s predictions. This means that the performance of the Maximum Softmax Probability (MSP) [15] method for OOD degrades with a greater number of classes. KL matching attempts to solve the class size problem by generating expected probability distributions around each category, a.k.a. posterior distribution templates, expecting in-distribution image patterns to more closely match the posterior distribution templates. In effect, it measures $P(\hat{y})$, the probability of the class existing in the in-distribution dataset.

However, KL matching has a major disadvantage compared to other methods; it needs to store the posterior distribution templates and use them for comparison. When performing OOD detection, each image’s predicted class distribution must be compared against each distribution template in order to find the minimum KL divergence value. This means that the computational cost scales with the square of the number of classes. Although this is not problematic with 1000 classes, it quickly becomes prohibitive when there are tens of thousands of classes or more.

3.3 Predicted Embedding Power Regression

In this work, we use the intuition behind KL matching to formulate a new conditional probability test that does not rely on an array of posterior distribution templates. Concretely, we consider the positive expectation of a model’s selected intermediate layer outputs conditioned on the predicted softmax probability distribution. Note that this test is crucially built on two key theoretical notions.

First, if a selected intermediate layer uses a linear rectifier based (ReLU-like) activation function followed by a batch normalization (batch norm) operation, that layer’s output can be viewed as an embedding z . A negative value in this layer’s

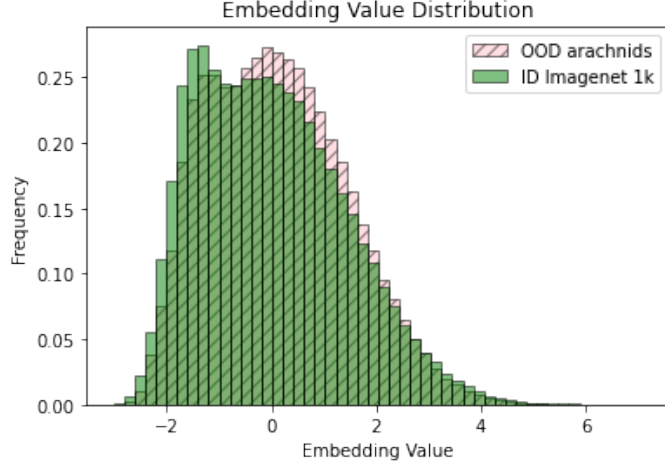


Figure 2: Distribution of embedding z for the OOD dataset *arachnids* compared to the in distribution dataset of Imagenet 1K. There is a noticeable tail in the distribution of the in-distribution dataset. These distributions overlap significantly. Frequency is such that the area sums to one.

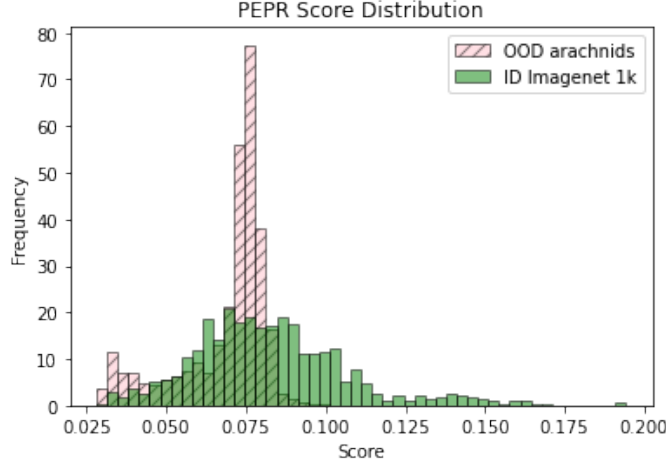


Figure 3: The distribution of $S_{\text{PEPR}}(x)$ for the OOD data *arachnids* compared to the Imagenet 1K in-distribution data. The regressor $\hat{z} = R(\hat{y})$ predicts significantly higher values for \hat{z} for in-distribution patterns when compared to OOD ones.

activity represents the absence of a feature and a positive value represents its presence. We observe empirically that such a layer, which precedes the final softmax classification output layer, exhibits a tail-heavy behaviour, with a large proportion of values below zero (the batch norm mean) and a minority of values significantly above zero. Figure 2 displays the distribution of embedding values of such a layer after model training. This means that, for any given image, we would expect to observe a minority consisting of very large positive values and a majority of consisting of negative values in z .

Second, an additional model, which we will refer to as the regressor $\hat{z} = R(\hat{y})$, will learn to predict the expected value of the embedding layer, i.e., $\mathbb{E}(z|\hat{y})$, where the predicted class distribution is $F(x) = \hat{y}$. When $R(\hat{y})$ is trained using a mean squared error loss, the regressor should learn to predict mostly negative values and a few large positive values. For class distributions that are not present in the training data, we would expect $R(\hat{y})$ to predict values close to zero, which is the true batch normalized mean for the embedding unconditional of the class, i.e., $\mathbb{E}(z) = 0$.

Combining the above two notions together yields our proposed OOD detection method, i.e., the predicted embedding power regression (PEPR) model. By using an intermediate layer between the model backbone and the softmax classification layer, PEPR can then focus on modeling a batch normalized embedding. We then train a nonlinear regression model to estimate the embedding values based on the softmax classification distribution. Note that we expect that the average of the squared positive expected embedding values to be higher for in-distribution data than for OOD data. In effect, we recover an estimate of $P(\hat{y})$ via the magnitude of \hat{z} , which is learned via regressor $R(\hat{y})$ from training data patterns. Note that our method only

adds a small amount of computational overhead. The actual score computed using our regressor is formally:

$$S_{\text{PEPR}}(x) = \frac{1}{n} \sum_{i=1}^n \left(\text{ReLU}(R(\hat{y})_i) \right)^2 \quad (2)$$

where n is the dimensionality of the embedding. An empirical sample of the PEPR score distribution is presented in Figure 3, which corroborates our hypothesis.

Finally, we further improve the PEPR model by also utilizing the actual embedding values. Specifically, we compute the actual embedding in-distribution score by calculating the mean of the squared embedding values, which we call the embedding power (EPOW). We then add this score, weighted by the coefficient parameter ψ , to the PEPR score and refer to the final score as C-PEPR. Formally, this score is calculated as follows:

$$S_{\text{C-PEPR}}(x) = S_{\text{PEPR}}(x) + \psi \frac{1}{n} \sum_{i=1}^n (z_i)^2 \quad (3)$$

Note that, in this work, we set the factor $\psi = 0.01$.

3.3.1 Stability

Our empirical results indicated that the PEPR and C-PEPR methods have a higher standard deviation than contemporary methods. Our methods tend to have a standard deviation of ≈ 0.9 AUROC, while MSP [15] and Minimum Other Score (MOS) [18] have a standard deviation of less than 0.1 AUROC. We decided to evaluate a 10 regressor ensemble of C-PEPR (C-PEPR-10) and a 10 classifier ensemble of MOS (MOS-10) to investigate the stability and AUROC improvements of ensembling.

3.3.2 Grouped Labels

In this paper, we train CPEPR and PEPR using the grouped softmax approach presented in [18]. Experimental results indicated that PEPR did not work quite as well with the standard softmax setup (average AUROC 78.4 vs 84.2). Detailed results for PEPR using standard softmax will be provided in the supplementary material. We believe that this issue may be caused by the high level of sparsity in the softmax probability values. Another possible explanation for this issue is that the learned embeddings are better when using the grouped softmax approach. Either way, grouped softmax PEPR achieves state of the art performance.

3.3.3 Bayesian Ensembling

Notably, we integrated the anchored ensembling approach presented in [31]. This scheme functions almost identically to L2 regularization of model weights, except that the regularization target is the random initial weight values rather than zero (as done in traditional parameter regularization, which assumes a zero-mean Gaussian prior over parameters). By taking an ensemble of networks regularized in this manner, Pearce [31] demonstrated that one can emulate the desired behaviour of a Bayesian neural network (without the prohibitive cost). While initially we intended to utilize Bayesian behaviour for OOD, PEPR and C-PEPR often worked quite well with an ensemble size of one. However, whether or not the regressor $R(\hat{y})$ is ensembled, our scoring models do require anchored regularization in order to achieve the best results presented as presented in Section 4.

Note that the anchored regularization scheme is only applied to our regressor $R(\hat{y})$ and not to the model classifier, embedding component, or model backbone. Equation 4 describes the anchored mean squared error loss for the j th (regressor) model for batches of size N with weights θ_j and initial weight values $\theta_{\text{anc},j}$.

$$\text{Loss}_j = \frac{1}{N} \|\mathbf{z} - \hat{\mathbf{z}}_j\|_2^2 + \frac{1}{N} \|\gamma \cdot (\theta_j - \theta_{\text{anc},j})\|_2^2 \quad (4)$$

We note that \hat{z}_j is the predicted value of z from the j th regressor model $R_j(\hat{y})$. We treat γ as a hyper-parameter and set it to 0.03 for all experiments unless otherwise specified.

4 Experiments

We provide a Github repository to fully replicate the experiments. We also provide Colab notebooks to allow users without access to local compute resources to run the experiments for themselves.



Figure 4: Samples of in-distribution/OOD data (as in [18]).

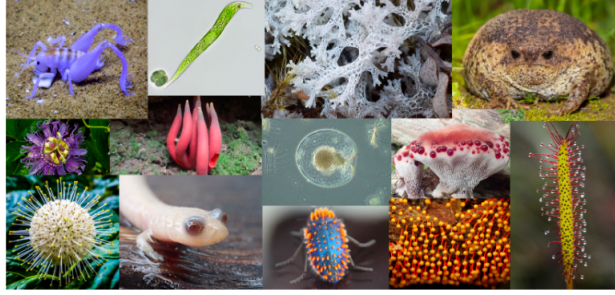


Figure 5: Samples from OOD datasets, as in [13]. Images extracted from the all species datasets.

4.1 Datasets

4.1.1 In-Distribution Dataset

We use Imagenet 1k as our in-distribution dataset [8]. This dataset has been used for large-scale OOD experiments such as those conducted by [18] and [13], which allows us to properly compare methods.

4.1.2 Out-of-Distribution Datasets

We used two sets of out-of-distribution (OOD) datasets. First is curated version of Textures, SUN, Places, and iNaturalist benchmarks, presented in [18]. Second, is the the Anomalous Species Dataset, presented in [13].

iNaturalist: iNaturalist [35] contains 859,000 images of 5,000 species of plants and animals. [18] manually selected 110 plant classes not present in ImageNet-1k and randomly sampled 10,000 images from these 110 classes. All images were resized to have a maximum dimension of 800 pixels.

SUN: SUN [37] is a scene database of 397 categories across 130,519 images with sizes larger than 200×200 . We used the curated version presented by [18], which randomly selected 10,000 images from 50 concepts not in ImageNet 1k.

Textures: Textures [5] consists of 5,640 images of textural patterns, with sizes ranging between 300×300 and 640×640 . Huang [18] uses the full dataset.

Places: Places365 [38] is a scene dataset that is similar to SUN. [18] resized all of the images to have a minimum dimension of 512. They [18] randomly selected 10,000 images from 50 concepts not in ImageNet 1k. It is unclear why [18] curated Places365 while [13] used Places365 without curation as the OOD set for Imagenet 1k.

Anomalous Species Dataset: The Species dataset [13] contains 700,000 species from the [35] dataset that do not overlap with Imagenet 21k [33]. Due to the quantity of images, we limit each species group to 12,800 images, with the exception of the micro-organisms group, where we use only 1,408 images due to the lack of images.

4.2 PEPR Embedder and Regressor

Unlike other OOD detection methods, PEPR requires a learnable intermediate layer to generate embeddings z and a regression model to estimate the embedding conditioned on the predicted softmax probability, i.e., $\hat{z} = R(\hat{y})$. Unless specified otherwise, the embedding model and regressor models are feedforward neural networks (FNNs) – the embedding FNN is specified in Listing 1 while the regressor FNN is specified in Listing 2. Note that only the embedding model’s outputs are used as input to the (softmax) classifier, while other methods use the backbone’s outputs directly as inputs to the classifier. Furthermore, the regressor $R(\hat{y})$ gradients must not flow to the embedding or classifier FNN modules. The interaction between these components is visualized in Figure 1.

Listing 1: Embedding Model

```
tf.keras.Sequential([
    Dense(512, activation='elu'),
    BatchNormalization(),
    Dropout(0.1),
    Dense(512, activation='elu'),
    BatchNormalization(),
    Dropout(0.1),
    Dense(256, activation='elu'),
    BatchNormalization()])
```

Listing 2: Regression Model

```
tf.keras.Sequential([
    Dense(512, activation='tanh'),
    Dense(256, activation='tanh'),
    Dense(256, activation=None),
    LeakyReLU(0.1)])
```

4.3 Experiment Setup

Pre-trained Backbone: Similar to [18], we use the Google BiT-S-R101x1 model [21] with a depth of 101 and width factor of one. Pre-trained models facilitate the extraction of high-quality features with minimal time and energy consumption. We choose to fix the backbone of our system and only train the final layers for each method investigated.

Pre-Computed Backbone Outputs: Due to the significant number of trials required for our experiments, we decided to significantly reduce energy consumption (and thus our computational carbon footprint) by pre-computing the backbone’s outputs and then re-using these for downstream simulation. Specifically, we pre-computed over 12 million backbone output vectors for Imagenet 1k, ensuring that each image contained multiple augmented backbone outputs. On a TPUv2-8 at batch size 512, pre-computed backbone outputs require ≈ 115 milliseconds (ms) for one training step while computing the backbone outputs during training requires ≈ 952 ms for one training step (due to memory limits, we must use gradient accumulation when computing backbone values). This is a 80% reduction in training time which results in a significant reduction in electricity usage and thus green house gas emissions. To ensure validity, we calculate the validation and OOD testing steps by calculating the backbone outputs at validation and test time, i.e., we run the model with input images during validation/testing.

Training Details: All models are trained using the Adam optimizer [20] with a step size of 0.0003 until the 9th epoch, where the learning rate is decreased by 40% (and again in the 10th epoch). We train for 10 epochs with batches of 512 samples and 1000 steps per epoch, i.e., a total of 10k steps. We decided that the BIT Hyperrule [21] does not apply if we choose to freeze the backbone or use pre-computed backbone outputs. When pre-computing backbone outputs, all images are resized to 512×512 and randomly cropped to 480×480 (using a random horizontal flip). At test time, all images are resized to 480×480 . At both pre-computing and test time, images are normalized as in [21]. We perform all experiments using TPUv2-8s on Google Colab.

Evaluation Metrics: We measure the following metrics commonly used in OOD detection: (1) the false positive rate of OOD examples when the true positive rate of in-distribution examples is at 95% (FPR95); (2) the area under the receiver operating characteristic curve (AUROC); and (3) the area under the precision-recall curve (AUPR). Note that we run each experiment 10 times and report the mean and standard deviation of the measurements.

We note that the KL matching method described by [13] calculated the posterior distribution templates using the in-distribution dataset labels. This can be problematic if we consider an in-distribution dataset with one image per class. In such a case, the KL divergence of each image’s predicted distribution versus the distribution templates would be minimal (as they would be the same values). To address this issue, we calculate the posterior distribution templates using the training data itself. We believe this to be an accurate representation of the KL matching method as [13] noted that the in-distribution dataset labels are not necessary for the KL matching method. For the above reasons, we recommend future researchers calculate KL matching without using the in-distribution test dataset labels.

Method	AUROC	AUPR	FPR95
	Mean $\pm \sigma$	Mean $\pm \sigma$	Mean $\pm \sigma$
C-PEPR (ours)	84.2 ± 0.9	96.2 ± 0.3	56.9 ± 1.3
C-PEPR-10 (ours)	84.6 ± 0.8	96.3 ± 0.3	57.0 ± 1.1
EPOW	74.9 ± 0.8	93.4 ± 0.2	75.7 ± 1.8
KLM	78.9 ± 0.1	93.4 ± 0.0	70.0 ± 0.2
MLGT	73.0 ± 0.1	92.7 ± 0.0	90.0 ± 0.1
MOS	82.4 ± 0.1	93.7 ± 0.0	52.5 ± 0.2
MOS-10	82.6 ± 0.0	93.7 ± 0.0	52.1 ± 0.1
MSP	78.3 ± 0.1	94.0 ± 0.0	77.7 ± 0.2
PEPR (ours)	82.5 ± 0.9	95.8 ± 0.3	57.4 ± 1.0
PEPR-10 (ours)	83.5 ± 0.8	96.1 ± 0.2	57.3 ± 0.9

Table 1: Summary of key statistics across runs. Mean and standard deviation (σ) reported across experimental runs. Values are calculated by first taking the mean metric across all datasets for a single experimental run, then calculating the mean and σ of the per-run metric across the 10 trials. Below is the legend for the method names.

- CPEPR: see Equation 3
- CPEPR-10: average of Equation 3 via 10 regressors
- EPOW: $S(x) = \psi \frac{1}{n} \sum_i^n (z_i)^2$
- KLM: KL Matching [13]
- MLGT: Max Logit [13]
- MOS: Minimum Other Score [18]
- MOS-10: Average of MOS across 10 classifiers
- MSP: Maximum Softmax Probability [15]
- PEPR: see Equation 2
- PEPR-10: average of Equation 2 via 10 regressors

5 Results

5.1 CPEPR versus Existing Methods:

We summarize mean results with variance across runs in Table 1. We compare with competitive methods in the literature that also do not rely on auxiliary outlier data. We include methods tested on large datasets, including MSP [15], MOS [18], KL matching [13], and Max Logit [13]. These methods, except for MOS, are trained using a flat, non-grouped, softmax. MOS is trained using grouped softmax, which uses the 8-class groups of [18].

Desirably, C-PEPR outperforms all other methods in terms of AUROC and AUPR by at least 1 standard deviation. It does perform worse than MOS in terms of FPR95, but it should be noted that FPR95 measures the false positive rate at an arbitrary recall level. The AUROC curve provides a better representation of the false positive rate at all recall levels. C-PEPR also maintains the same execution speed characteristics as MOS as it only needs to compute a few extra fully-connected layers. Using the embedding FNN resulted in a slightly lower validation classification accuracy compared with MOS (≈ 75.1 versus ≈ 77.4). However, this does not seem to negatively affect the OOD detection performance of the model.

5.2 On the Bias-Variance Tradeoff:

Compared with MOS, PEPR and CPEPR appear to benefit more from a 10-fold ensemble. PEPR-10 is 1 standard deviation better than MOS-10, but PEPR is not statistically different from MOS, in terms of AUROC. We believe that this is due to the greater standard deviation across all metrics for PEPR and CPEPR. Compared with other OOD methods, our method appears to reduce bias at the expense of increased variance. This is much more noticeable when analyzing results for specific datasets. However, when we consider variance across datasets, PEPR and CPEPR have lower AUROC (11.0 vs 13.2) and AUPR (2.7 vs 5.8) standard deviation than MOS. This suggests that the our method performs more consistently across datasets. Overall, this is an advantage that allows users to choose between efficiency and accuracy.

5.3 On Issues with Benchmark Selection:

We can clearly observe that OOD methods vary greatly in performance across different datasets. For example, in Table 2, KL Matching outperforms MOS by a significant margin for amphibians, fish, and mammals. If [18] decided to include these three species benchmarks in their paper, MOS would perform worse than KL Matching in terms of AUROC (79.6 versus 80.0). If we only evaluated our methods (PEPR & C-PEPR) using only the four benchmarks provided by [18], then

our AUROC performance would not exceed the state-of-the-art (81.2 versus 89.6). As such, evaluation of OOD detection methods may suffer from a definition problem. While researchers agree on the definition of a single out-of-distribution image, they may not agree on the relative weighting of out-of-distribution benchmarks.

Should a researcher consider anomalous species [13] as one dataset, equal in weight to the Places benchmark? We elected to treat anomalous species as multiple out-of-distribution datasets in order to follow precedent set by [13], but we note that this more heavily weights the images in the anomalous species dataset. The choice of out-of-distribution datasets greatly affects the performance of OOD detection methods. This stands in contrast to other machine learning research areas, such as image classification, where improvements in one dataset often correlate with improvements in another.

The issue of benchmark selection is not only limited to selecting the out-of-distribution datasets. Recent work by [10] showed that they have achieved effectively the ideal AUROC on CIFAR10 versus CIFAR100. It is unclear, however, whether or not their approach would outperform contemporary large-scale OOD methods. In light of the above issues, we encourage further research into OOD benchmark design so that the community may progress towards a consensus on which benchmarks should be used (and the nature in how they are used) for evaluation.

5.4 Poor Performance on the Textures Dataset:

Detailed results for each dataset are presented in the Table 2. CPEPR and PEPR perform very poorly (<60 AUROC) on the textures dataset, which may be explained by the poor performance of the EPOW method. This would suggest that PEPR is limited/hindered by EPOW performance; the usefulness of the estimate of the embeddings is affected by the very embeddings themselves. However, this hypothesis does not apply for the micro-organisms dataset, in which PEPR achieves more than 80 AUROC and EPOW achieves less than 55 AUROC. This phenomenon warrants further investigation by future researchers.

5.5 On Efficient Evaluation and Reproduction:

We compare our results for contemporary methods with those from [18] using their four datasets. Our pre-computed backbone outputs setup (see Section 4.3) differs from previous approaches/setups but reduces training time by 80%, which results in a significant reduction in electricity usage and thus green house gas emissions. We see that our reproduction of MOS method achieves an average AUROC across the four datasets (Textures, SUN, Places, iNaturalist) of 89.6 versus the 90.1 reported in the original paper [18]. We also observe a better average FPR95 of 38.8 versus 40.0 on the same four datasets for the MOS method. We believe that our experimental setup faithfully represents MOS and other contemporary methods while significantly reducing the carbon footprint via pre-computed backbone outputs and fewer require training steps.

6 Conclusion

In this work, we proposed a novel OOD detection method, predicted embedding power regression (PEPR), motivated by the properties of intermediate neural layer embeddings. Our experimental results indicate that PEPR performs well for the case of large-scale OOD detection. We train PEPR and other contemporary methods using pre-computed outputs, significantly reducing compute costs. Our experiments across a wide array of datasets shows the PEPR performs better than the state of the art in a statistically significant way. We hope that our study encourages further research in large-scale OOD detection and provides machine learning practitioners with new tools to improve artificial intelligence safety.

Acknowledgements

This material is based upon work supported by the United States National Science Foundation under grant #2225354

Method Dataset AUROC	<i>C-PEPR</i>	<i>C-PEPR-10</i>	<i>EPOW</i>	<i>KLM</i>	<i>MLGT</i>	<i>MOS</i>	<i>MOS-10</i>	<i>MSP</i>	<i>PEPR</i>	<i>PEPR-10</i>
Places	85.9 ±1.9	86.1 ±1.9	83.7 ±0.8	78.4 ±0.1	78.2 ±0.1	89.7 ±0.1	89.8 ±0.1	78.2 ±0.1	83.9 ±1.7	84.2 ±1.7
SUN	87.9 ±2.0	88.1 ±2.0	84.3 ±0.8	81.5 ±0.1	78.3 ±0.1	92.5 ±0.1	92.6 ±0.0	80.2 ±0.1	86.2 ±1.9	86.5 ±1.8
Textures	56.0 ±2.8	55.7 ±2.4	50.0 ±1.6	83.2 ±0.1	68.0 ±0.1	78.7 ±0.4	78.9 ±0.1	76.9 ±0.1	57.8 ±3.2	58.1 ±2.4
amphibians	72.2 ±4.7	72.1 ±4.4	61.3 ±2.7	72.1 ±0.2	68.6 ±0.1	59.1 ±0.3	59.2 ±0.1	75.0 ±0.1	69.9 ±4.8	68.5 ±4.9
arachnids	82.0 ±3.7	83.2 ±2.5	76.2 ±1.5	69.5 ±0.1	59.0 ±0.2	67.5 ±0.3	67.7 ±0.2	76.7 ±0.1	78.7 ±5.3	82.1 ±3.4
fish	84.1 ±2.4	85.3 ±2.2	78.8 ±1.7	79.5 ±0.2	73.2 ±0.1	72.9 ±0.4	72.9 ±0.2	78.4 ±0.1	80.1 ±2.4	83.2 ±2.5
fungi	96.7 ±0.4	96.7 ±0.3	86.6 ±1.5	73.4 ±0.2	67.0 ±0.2	93.1 ±0.1	93.4 ±0.1	73.4 ±0.2	96.1 ±0.5	96.0 ±0.4
iNaturalist	94.8 ±0.4	94.8 ±0.3	82.5 ±1.8	89.9 ±0.1	81.5 ±0.1	97.5 ±0.1	97.5 ±0.0	86.5 ±0.1	94.0 ±0.5	94.2 ±0.3
insects	82.4 ±3.4	83.3 ±2.8	78.7 ±1.4	67.7 ±0.1	63.5 ±0.1	73.1 ±0.3	73.3 ±0.1	72.5 ±0.1	77.2 ±4.4	78.5 ±3.6
mammals	76.1 ±2.5	76.2 ±2.8	65.6 ±1.2	75.4 ±0.1	71.5 ±0.1	66.9 ±0.2	67.2 ±0.1	77.5 ±0.1	74.0 ±2.7	73.7 ±2.6
microorganisms	86.4 ±1.5	87.0 ±1.3	54.1 ±4.1	89.0 ±0.6	80.9 ±0.6	93.5 ±0.2	93.7 ±0.1	81.7 ±0.7	87.4 ±1.5	88.8 ±1.3
mollusks	82.5 ±2.8	84.3 ±1.9	74.0 ±1.6	69.8 ±0.2	69.2 ±0.2	75.7 ±0.3	75.8 ±0.1	69.5 ±0.1	79.9 ±3.5	84.4 ±1.9
plants	95.7 ±0.4	95.7 ±0.5	88.6 ±1.2	91.5 ±0.1	83.0 ±0.1	98.0 ±0.0	98.0 ±0.0	88.5 ±0.1	94.6 ±0.6	94.7 ±0.7
protozoa	96.1 ±0.3	96.2 ±0.2	84.7 ±1.8	83.7 ±0.1	80.8 ±0.1	95.7 ±0.1	95.9 ±0.0	81.5 ±0.1	95.5 ±0.4	95.7 ±0.3
Dataset AUPR										
Places	96.2 ±0.6	96.3 ±0.5	96.0 ±0.2	94.3 ±0.0	94.9 ±0.0	97.0 ±0.0	97.1 ±0.0	94.5 ±0.0	95.4 ±0.5	95.6 ±0.5
SUN	96.7 ±0.6	96.8 ±0.5	95.8 ±0.3	95.0 ±0.0	95.0 ±0.0	98.0 ±0.0	98.0 ±0.0	95.0 ±0.0	96.1 ±0.6	96.3 ±0.5
Textures	90.9 ±0.7	90.7 ±0.5	89.2 ±0.6	97.2 ±0.0	95.1 ±0.0	95.9 ±0.1	96.0 ±0.0	96.3 ±0.0	92.0 ±0.8	92.2 ±0.5
amphibians	92.4 ±1.6	92.4 ±1.6	86.4 ±1.4	90.2 ±0.1	89.9 ±0.1	83.0 ±0.1	83.1 ±0.1	92.6 ±0.0	91.9 ±1.6	91.5 ±1.6
arachnids	95.6 ±1.2	96.0 ±0.9	92.7 ±0.6	90.3 ±0.0	87.7 ±0.1	88.0 ±0.1	88.1 ±0.1	93.2 ±0.1	94.9 ±1.6	95.8 ±0.9
fish	95.9 ±0.7	96.3 ±0.6	93.4 ±0.7	93.7 ±0.1	92.3 ±0.1	89.3 ±0.2	89.3 ±0.1	93.7 ±0.0	94.8 ±0.7	95.7 ±0.7
fungi	99.2 ±0.1	99.2 ±0.1	96.2 ±0.5	90.8 ±0.1	89.5 ±0.1	97.4 ±0.1	97.5 ±0.0	91.2 ±0.1	99.0 ±0.1	99.0 ±0.1
iNaturalist	98.9 ±0.1	98.9 ±0.1	95.8 ±0.5	97.2 ±0.0	96.0 ±0.0	99.4 ±0.0	99.4 ±0.0	96.9 ±0.0	98.7 ±0.1	98.8 ±0.1
insects	95.4 ±1.1	95.7 ±0.8	93.5 ±0.5	87.0 ±0.1	87.4 ±0.1	89.0 ±0.1	89.0 ±0.0	91.1 ±0.1	93.8 ±1.5	94.3 ±1.1
mammals	93.2 ±1.0	93.2 ±1.2	87.5 ±0.6	91.2 ±0.1	90.8 ±0.1	86.3 ±0.1	86.4 ±0.0	92.3 ±0.0	92.7 ±1.0	92.7 ±0.9
microorganisms	99.5 ±0.1	99.5 ±0.1	97.6 ±0.4	99.6 ±0.0	99.4 ±0.0	99.7 ±0.0	99.7 ±0.0	99.3 ±0.0	99.5 ±0.1	99.6 ±0.1
mollusks	95.5 ±0.8	96.0 ±0.5	91.5 ±0.7	89.3 ±0.1	90.0 ±0.1	90.1 ±0.1	90.2 ±0.0	89.1 ±0.1	94.8 ±1.0	96.2 ±0.5
plants	98.8 ±0.1	98.8 ±0.2	96.8 ±0.4	97.6 ±0.0	95.7 ±0.0	99.5 ±0.0	99.5 ±0.0	96.8 ±0.0	98.5 ±0.2	98.6 ±0.3
protozoa	99.0 ±0.1	99.0 ±0.1	95.7 ±0.5	94.2 ±0.1	94.8 ±0.1	98.8 ±0.0	98.9 ±0.0	94.5 ±0.1	98.8 ±0.1	98.8 ±0.1
Dataset FPR95										
Places	37.0 ±1.1	37.1 ±0.9	65.1 ±2.3	76.8 ±0.2	84.2 ±0.2	44.0 ±0.2	43.6 ±0.2	78.8 ±0.2	38.0 ±1.0	38.0 ±1.0
SUN	32.1 ±1.0	32.2 ±0.8	56.2 ±2.0	71.5 ±0.2	87.2 ±0.1	35.5 ±0.4	35.1 ±0.2	74.5 ±0.3	33.1 ±1.0	33.0 ±0.9
Textures	77.3 ±0.5	77.4 ±0.4	90.8 ±0.7	62.4 ±0.4	93.7 ±0.2	64.5 ±0.4	64.7 ±0.2	78.9 ±0.3	76.2 ±0.6	76.1 ±0.6
amphibians	91.1 ±1.1	91.2 ±1.0	92.8 ±1.2	81.3 ±0.2	88.1 ±0.2	86.7 ±0.2	86.6 ±0.1	83.7 ±0.3	91.5 ±0.8	91.5 ±0.8
arachnids	91.0 ±1.6	91.2 ±1.3	77.2 ±3.1	88.4 ±0.2	96.6 ±0.1	87.5 ±0.4	87.5 ±0.1	87.2 ±0.2	92.1 ±1.0	92.1 ±0.9
fish	79.4 ±2.7	79.5 ±2.4	77.2 ±2.6	81.9 ±0.3	92.6 ±0.1	84.3 ±0.5	84.2 ±0.2	84.4 ±0.3	80.7 ±2.2	80.7 ±2.0
fungi	11.9 ±2.5	11.9 ±2.0	64.4 ±4.8	84.1 ±0.3	94.7 ±0.1	27.2 ±0.6	26.2 ±0.2	87.3 ±0.2	14.6 ±3.2	14.3 ±2.4
iNaturalist	27.2 ±2.9	27.4 ±2.5	70.6 ±4.1	45.6 ±0.3	88.8 ±0.2	11.2 ±0.3	10.8 ±0.1	61.9 ±0.4	29.1 ±3.1	28.9 ±2.7
insects	84.8 ±2.4	85.0 ±2.0	78.9 ±2.7	79.0 ±0.2	92.2 ±0.1	75.5 ±0.4	75.4 ±0.2	84.2 ±0.3	86.0 ±1.8	86.1 ±1.6
mammals	85.4 ±1.3	85.5 ±1.1	88.5 ±1.3	72.1 ±0.2	84.9 ±0.1	81.9 ±0.2	81.7 ±0.1	75.0 ±0.3	85.9 ±1.0	86.0 ±1.0
microorganisms	56.5 ±4.4	56.9 ±4.3	89.5 ±0.7	44.8 ±1.1	92.8 ±0.3	28.7 ±1.1	27.3 ±0.3	70.5 ±1.5	48.0 ±3.6	48.1 ±3.5
mollusks	83.7 ±2.4	83.9 ±2.1	82.9 ±1.9	80.1 ±0.2	91.1 ±0.1	73.7 ±0.3	73.4 ±0.1	85.6 ±0.2	84.8 ±1.8	84.9 ±1.7
plants	22.1 ±2.2	22.3 ±1.8	54.9 ±4.3	46.4 ±0.7	85.6 ±0.2	9.1 ±0.3	8.6 ±0.1	59.9 ±1.0	25.5 ±2.8	25.3 ±2.3
protozoa	16.5 ±1.9	16.6 ±1.6	70.1 ±5.0	65.3 ±0.6	87.8 ±0.1	25.1 ±0.7	24.2 ±0.3	75.2 ±0.4	17.8 ±1.8	17.6 ±1.5

Table 2: AUROC, AUPR, and FPR95 Results for All Datasets expressed as MEAN±σ. See table 1 for method descriptions

References

- [1] Johnathan M Bardsley, Antti Solonen, Heikki Haario, and Marko Laine. Randomize-then-optimize: A method for sampling from posterior distributions in nonlinear inverse problems. *SIAM Journal on Scientific Computing*, 36(4):A1895–A1910, 2014. 2
- [2] Petra Bevanđić, Ivan Krešo, Marin Oršić, and Siniša Šegvić. Discriminative out-of-distribution detection for semantic segmentation. *arXiv preprint arXiv:1808.07703*, 2018. 1, 2
- [3] Daniel Bogdoll, Maximilian Nitsche, and J Marius Zöllner. Anomaly detection in autonomous driving: A survey. In *Proceedings of the IEEE/CVF conference on computer vision and pattern recognition*, pages 4488–4499, 2022. 1
- [4] Yan Chen and Dean S Oliver. Ensemble randomized maximum likelihood method as an iterative ensemble smoother. *Mathematical Geosciences*, 44:1–26, 2012. 2
- [5] Mircea Cimpoi, Subhransu Maji, Iasonas Kokkinos, Sammy Mohamed, and Andrea Vedaldi. Describing textures in the wild. In *Proceedings of the IEEE conference on computer vision and pattern recognition*, pages 3606–3613, 2014. 6
- [6] Djork-Arné Clevert, Thomas Unterthiner, and Sepp Hochreiter. Fast and accurate deep network learning by exponential linear units (elus). *arXiv preprint arXiv:1511.07289*, 2015. 1
- [7] Jia Deng, Nan Ding, Yangqing Jia, Andrea Frome, Kevin Murphy, Samy Bengio, Yuan Li, Hartmut Neven, and Hartwig Adam. Large-scale object classification using label relation graphs. In *Computer Vision–ECCV 2014: 13th European Conference, Zurich, Switzerland, September 6–12, 2014, Proceedings, Part I 13*, pages 48–64. Springer, 2014. 2
- [8] Jia Deng, Wei Dong, Richard Socher, Li-Jia Li, Kai Li, and Li Fei-Fei. Imagenet: A large-scale hierarchical image database. In *2009 IEEE conference on computer vision and pattern recognition*, pages 248–255. Ieee, 2009. 1, 2, 6
- [9] Jia Deng, Sanjeev Sathesh, Alexander Berg, and Fei Li. Fast and balanced: Efficient label tree learning for large scale object recognition. *Advances in Neural Information Processing Systems*, 24, 2011. 2
- [10] Stanislav Fort, Jie Ren, and Balaji Lakshminarayanan. Exploring the limits of out-of-distribution detection. *Advances in Neural Information Processing Systems*, 34:7068–7081, 2021. 9
- [11] Yonatan Geifman and Ran El-Yaniv. Selectivenet: A deep neural network with an integrated reject option. In *International conference on machine learning*, pages 2151–2159. PMLR, 2019. 2
- [12] Sam Gross, Marc’Aurelio Ranzato, and Arthur Szlam. Hard mixtures of experts for large scale weakly supervised vision. In *Proceedings of the IEEE Conference on Computer Vision and Pattern Recognition*, pages 6865–6873, 2017. 2
- [13] Dan Hendrycks, Steven Basart, Mantas Mazeika, Mohammadreza Mostajabi, Jacob Steinhardt, and Dawn Song. Scaling out-of-distribution detection for real-world settings. *arXiv preprint arXiv:1911.11132*, 2019. 1, 2, 3, 6, 7, 8, 9
- [14] Dan Hendrycks, Nicholas Carlini, John Schulman, and Jacob Steinhardt. Unsolved problems in ml safety. *arXiv preprint arXiv:2109.13916*, 2021. 1
- [15] Dan Hendrycks and Kevin Gimpel. A baseline for detecting misclassified and out-of-distribution examples in neural networks. *arXiv preprint arXiv:1610.02136*, 2016. 1, 2, 3, 5, 8
- [16] Dan Hendrycks, Mantas Mazeika, and Thomas Dietterich. Deep anomaly detection with outlier exposure. *arXiv preprint arXiv:1812.04606*, 2018. 1, 2
- [17] Geoffrey Hinton, Oriol Vinyals, and Jeff Dean. Distilling the knowledge in a neural network. *arXiv preprint arXiv:1503.02531*, 2015. 2
- [18] Rui Huang and Yixuan Li. Mos: Towards scaling out-of-distribution detection for large semantic space. In *Proceedings of the IEEE/CVF Conference on Computer Vision and Pattern Recognition*, pages 8710–8719, 2021. 1, 2, 5, 6, 7, 8, 9
- [19] Sergey Ioffe and Christian Szegedy. Batch normalization: Accelerating deep network training by reducing internal covariate shift. In *International conference on machine learning*, pages 448–456. pmlr, 2015. 1
- [20] Diederik Kingma and Jimmy Ba. Adam: A method for stochastic optimization. *arXiv preprint arXiv:1412.6980*, 2014. 7
- [21] Alexander Kolesnikov, Lucas Beyer, Xiaohua Zhai, Joan Puigcerver, Jessica Yung, Sylvain Gelly, and Neil Houlsby. Big transfer (bit): General visual representation learning. In *Computer Vision–ECCV 2020: 16th European Conference, Glasgow, UK, August 23–28, 2020, Proceedings, Part V 16*, pages 491–507. Springer, 2020. 2, 7
- [22] Balaji Lakshminarayanan, Alexander Pritzel, and Charles Blundell. Simple and scalable predictive uncertainty estimation using deep ensembles. *Advances in neural information processing systems*, 30, 2017. 1, 2
- [23] Kimin Lee, Honglak Lee, Kibok Lee, and Jinwoo Shin. Training confidence-calibrated classifiers for detecting out-of-distribution samples. *arXiv preprint arXiv:1711.09325*, 2017. 2
- [24] Kimin Lee, Kibok Lee, Honglak Lee, and Jinwoo Shin. A simple unified framework for detecting out-of-distribution samples and adversarial attacks. *Advances in neural information processing systems*, 31, 2018. 2
- [25] Shiyu Liang, Yixuan Li, and Rayadurgam Srikant. Enhancing the reliability of out-of-distribution image detection in neural networks. *arXiv preprint arXiv:1706.02690*, 2017. 1, 2
- [26] Weitang Liu, Xiaoyun Wang, John Owens, and Yixuan Li. Energy-based out-of-distribution detection. *Advances in neural information processing systems*, 33:21464–21475, 2020. 2
- [27] Xiuyuan Lu and Benjamin Van Roy. Ensemble sampling. *Advances in neural information processing systems*, 30, 2017. 2
- [28] Andrey Malinin and Mark Gales. Predictive uncertainty estimation via prior networks. *Advances in neural information processing systems*, 31, 2018. 2
- [29] Gustav Mårtensson, Daniel Ferreira, Tobias Granberg, Lena Cavallin, Ketil Oppedal, Alessandro Padovani, Irena Rektorova, Laura Bonanni, Matteo Pardini, Milica G Kramberger, et al. The reliability of a deep learning model in clinical out-of-distribution mri data: a multicohort study. *Medical Image Analysis*, 66:101714, 2020. 1
- [30] Sina Mohseni, Mandar Pitale, JBS Yadawa, and Zhangyang Wang. Self-supervised learning for generalizable out-of-distribution detection. In *Proceedings of the AAAI Conference on Artificial Intelligence*, volume 34, pages 5216–5223, 2020. 2
- [31] Tim Pearce, Felix Leibfried, and Alexandra Brintrup. Uncertainty in neural networks: Approximately bayesian ensembling. In *International conference on artificial intelligence and statistics*, pages 234–244. PMLR, 2020. 2, 5
- [32] Joseph Redmon and Ali Farhadi. Yolo9000: better, faster, stronger. In *Proceedings of the IEEE conference on computer vision and pattern recognition*, pages 7263–7271, 2017. 2

- [33] Tal Ridnik, Emanuel Ben-Baruch, Asaf Noy, and Lihi Zelnik-Manor. Imagenet-21k pretraining for the masses. *arXiv preprint arXiv:2104.10972*, 2021. 1, 6
- [34] Ryne Roady, Tyler L Hayes, Ronald Kemker, Ayesha Gonzales, and Christopher Kanan. Are out-of-distribution detection methods effective on large-scale datasets? *arXiv preprint arXiv:1910.14034*, 2019. 2
- [35] Grant Van Horn, Oisín Mac Aodha, Yang Song, Yin Cui, Chen Sun, Alex Shepard, Hartwig Adam, Pietro Perona, and Serge Belongie. The inaturalist species classification and detection dataset. In *Proceedings of the IEEE conference on computer vision and pattern recognition*, pages 8769–8778, 2018. 6
- [36] David Warde-Farley, Andrew Rabinovich, and Dragomir Anguelov. Self-informed neural network structure learning. *arXiv preprint arXiv:1412.6563*, 2014. 2
- [37] Jianxiong Xiao, James Hays, Krista A Ehinger, Aude Oliva, and Antonio Torralba. Sun database: Large-scale scene recognition from abbey to zoo. In *2010 IEEE computer society conference on computer vision and pattern recognition*, pages 3485–3492. IEEE, 2010. 6
- [38] Bolei Zhou, Agata Lapedriza, Aditya Khosla, Aude Oliva, and Antonio Torralba. Places: A 10 million image database for scene recognition. *IEEE transactions on pattern analysis and machine intelligence*, 40(6):1452–1464, 2017. 6